

Numerical experiments of two-phase flow in pipelines with a two-fluid compressible model

P. Loilier, C. Omgba-Essama and C. Thompson

Applied Mathematics and Computing Group, School of Engineering, Cranfield University, Cranfield, Bedfordshire, MK43 0AL, England

Abstract

Getting an accurate understanding of the dynamics of multiphase transport for the design of efficient pipelines is an important issue in the oil and gas industry. This paper presents simulations of one-dimensional two-phase flow in pipelines. The compressible model used is derived from the two-fluid model where pressure relaxation terms are added. The governing system consists of five time-dependent partial differential equations solved explicitly by a finite volume approach. Numerical results on well-known air-water compressible flow problems are performed and analysed. Common problems are observed with coarse meshes and are reduced with mesh refinement. We conclude that the model and the discretisation each behave well in regions of large discontinuities of pressure and velocities.

Variables		Greek symbols	
a_k, c_k	Speed of sound	α_k	Volume fraction
F	Flux vector	ρ_k	Density
F^c	Convective flux	θ	Inclination angle
F^p	Pressure terms flux	μ	Dynamic compaction viscosity
H	Interface matrix	δ	Constant
M_k	Momentum transfer of phase k	χ_L	Near one-phase smoother
P_k	Pressure of phase k	ϕ	Near one-phase smoothing function
P^\pm	Split pressure function	Δx	Mesh size
S	Source terms vector	Δt	Time-step
T_k	Temperature of phase k	Subscripts-superscripts	
U	Vector of conservative variables of	j	Time indices
V_k	Velocity of phase k	k	Phase identifier
\bar{V}^\pm	Split velocity function	m	Mesh refinement level
		n	Space indices

Table 1: Nomenclature

1 INTRODUCTION

One of the big issues in the oil and gas industries is the understanding of the behaviour of multiphase mixtures in pipeline transport. Indeed, it is important to be able to predict the gas or oil production rate of a system, or to check the efficiency of a pipeline design. All of this information can be obtained by numerical simulation. Research on such predictions has been conducted for several years, and is still a major challenge today.

Mathematical models for predicting two-phase flows range from homogeneous models to multi-field models. Two-fluid models, obtained by averaging local field equations, enable both mechanical and thermal non-equilibrium to be taken into account, and represent a more general model than homogeneous models for two-phase flow. The two-fluid method assumes that both the continuous and dispersed phases can be represented as two separate, but inter-mixed continua. Therefore it accounts for relative interphase velocity and pressure differences. In a one-dimensional framework, the technique is to average the local instantaneous conservation laws (time-, space- or ensemble-averaged). This set of averaged equations can be written for each field (or fluid). This approach simplifies the mathematical aspects of the equations, but neglects some information about the local gradients at interfaces and walls. Therefore, additional correlations such as pressure and velocity at the interface are required in order to close the mathematical model.

Two-fluid models with an equilibrium pressure assumption have some drawbacks. In particular, they do not remain hyperbolic for the entire domain of calculation (the whole range of volume fraction), which leads to an initial value problem which is "ill-posed" for many initial conditions. Using a two-pressure approach will allow a formulation with the unconditional hyperbolicity of the system and this approach will remove instabilities which occur with other models. Different researchers (1... 6) have already presented some results of two-pressure based model on classical two-phase benchmarks. Their works differ by some variations in either the model formulation (1), (2) or the numerical method associated with (3), (6). The model presented in this work is based on a two-fluid model with two distinct pressures in which a relaxation stage at the interface is included. The computation process is thus divided into two: (a) solving the hyperbolic system assuming different pressures, followed by (b) a relaxation on the pressures towards equilibrium at the interface.

As far as numerical methods are concerned, the method used in this work describes the characteristic-based upwind differencing schemes detailed in (1), (6), (7). Many of them are categorised as flux difference splitting (FDS) and are based on Godunov-type schemes and Roe-type schemes. They are robust and accurate, but rather time-consuming since they are based on matrix calculations (8), (6). The flux vector splitting (FVS) method is based on scalar calculations, hence they are more efficient than FDS schemes on a per cell basis but they are also much more diffusive. During the last few years, many authors have worked on combining both methods: get the efficiency of FVS to the accuracy of FDS. These are called hybrid flux-splitting schemes and are commonly termed the Advection Upstream Splitting Methods (AUSM) family (9), (10). Evje and Flatten (3) have developed a hybrid scheme called AUSMDV*, which combines FVS/FDS schemes. The motivation for the choice of such schemes is their accuracy, robustness and non-oscillatory nature in their results of classical two-phase benchmarks, even when transition from two-phase to near single-phase regions occurs such as for the phase separation problem.

This paper is organised as follows: the second section will detail the formulation of the mathematical model, with the different closure relations required (thermodynamic, interface treatments...). The relaxation process is also explained in this section. Numerical method and the different discretisation schemes which we have used are described in the third section. In Section 4, classical two-fluid air-water test-cases simulations are presented and discussed. They have been chosen to assess the ability of the model for handling different situations: presence of source terms, transition from two-phase to one-phase regions, or discontinuities... Conclusions and future work are developed in the final section of the document.

2 TWO-FLUID MODEL

2.1 Governing equations

The model we investigate in this work assumes isothermal flow, allowing us to neglect the equations of energy. Hence the one-dimensional system governing two-phase compressible flows contains five time-dependent partial differential equations, four obtained from the conservation of mass and momentum for each phase. A fifth equation is added to the mass and momentum equations, which expresses the evolution of the volume fraction and is obtained by an averaging procedure (1), (2). The system can be expressed as:

$$\begin{aligned} \frac{\partial}{\partial t}(\alpha_k \rho_k) + \frac{\partial}{\partial x}(\alpha_k \rho_k V_k) &= 0 \\ \frac{\partial}{\partial t}(\alpha_k \rho_k V_k) + \frac{\partial}{\partial x}(\alpha_k (\rho_k V_k^2 + P_k)) &= P_i \frac{\partial}{\partial x} \alpha_k + M_k + \alpha_k \rho_k g \sin \theta \quad (k = g, l) \\ \frac{\partial}{\partial t} \alpha_g + V_i \frac{\partial}{\partial x} \alpha_g &= \mu (P_g - P_l) \end{aligned} \quad (1.1)$$

where α_k is the void fraction of phase k , ρ_k , V_k are the density and the velocity of phase k , ($k=g, l$). The mass fraction is defined $m_k = \alpha_k \rho_k$ and the pressure P_k of phase k . $V_i(U)$ and $P_i(U)$ represent the averaged values of the interfacial velocity and the interfacial pressure over the two-phase control volume, they must be modelled by closure laws. μ is the positive function of pressure relaxation. Terms M_g, M_l correspond to the gas and liquid phase momentum transfer and can be composed of the drag force effects.

The interface pressure condition under two pure fluids consists in pressure equality across the interface. During the resolution of the two-phase equations, the fluids mixed at the beginning and also at the interface with the numerical diffusion. Therefore to restore the interface pressure condition, it is necessary to impose pressure equality between phases. And since pressure equality must be satisfied at each time, the pressure relaxation has to be instantaneous, so that the dynamic compaction viscosity μ tends to infinity.

The variables are then evolved over time by solution of a strictly hyperbolic system, followed by a pressure relaxation step. This is different from the single-pressure models that solve a system where the pressure equilibrium is already assumed in the equations, leading to a system which is not hyperbolic for certain conditions and therefore this becomes a very difficult problem to solve for such cases. Additionally, the expression of the characteristics of a two-pressure model is far simpler than for the single-pressure models, simplifying the computations.

2.2 Thermodynamic equations of state

The system is closed by an equation of state (EOS) for the gas and liquid phases. In this work we will assume the simplified thermodynamic relations for both phases (see (3)):

$$\rho_k = \rho_{k,0} + \frac{P_k - P_{k,0}}{a_k^2} \quad (1.2)$$

The compressibilities are constant, given by:

$$\frac{\partial P_k}{\partial \rho_k} = \alpha_k^2. \quad (1.3)$$

And the following parameters are used for each phase:

$$P_{l,0} = 1 \text{ bar} = 10^5 \text{ Pa}, \quad \rho_{l,0} = 1000 \text{ kg/m}^3; \quad \alpha_l^2 = 10^6 \text{ (m/s)}^2, \text{ and}$$

$$P_{g,0} = 0 \text{ bar}; \quad \rho_{g,0} = 0 \text{ kg/m}^3; \quad \alpha_g^2 = 10^5 \text{ (m/s)}^2.$$

2.3 Interfacial relations

For the interface pressure P_i , the model we use is the one detailed by Bestion (12):

$$\Delta P = P_g - P_i = \delta \frac{\alpha_g \alpha_l \rho_g \rho_l}{\rho_g \alpha_l + \rho_l \alpha_g} (V_g - V_l)^2 \quad (1.4)$$

with $\delta = 2.0$. This choice ensures that the system is hyperbolic after the relaxation process.

3 NUMERICAL METHOD

The numerical scheme used in this work is based on the Advection Upstream Splitting Method (AUSM) approach (9), (10). Among the several schemes developed with this approach, we choose to concentrate on AUSMD* and AUSMV*. Both schemes derive from the AUSM schemes where D and V respectively denote flux-difference biased scheme and flux-vector biased scheme (3).

If we rewrite the system of governing equations (Eq 1.1) as

$$\frac{\partial U}{\partial t} + \frac{\partial F(U)}{\partial x} + H(U) \frac{\partial P_i}{\partial x} = S(U) \quad (1.5)$$

where U is the vector of conservative variables, $F(U)$ the numerical flux, $H(U)$ the interface matrix and $S(U)$ the vector of source terms, the finite volume discretisation gives

$$U_j^{n+1} = U_j^n + \frac{\Delta t}{\Delta x} (F_{j+1/2} - F_{j-1/2}) + \Delta t (H \frac{\partial P_i}{\partial x})_j^n + \Delta t S_j^n. \quad (1.6)$$

We can split the numerical flux F into a convective flux and a pressure term flux

$$F = F_{j+1/2}^c + F_{j+1/2}^p \quad (1.7)$$

where

$$F^c = \begin{bmatrix} \rho_g \alpha_g V_g \\ \rho_l \alpha_l V_l \\ \rho_g \alpha_g V_g^2 \\ \rho_l \alpha_l V_l^2 \end{bmatrix} = \begin{bmatrix} \text{gas mass flux} \\ \text{liquid mass flux} \\ \text{gas momentum flux} \\ \text{liq. momentum flux} \end{bmatrix} \quad \text{and} \quad F^p = \begin{bmatrix} 0 \\ 0 \\ \alpha_g \Delta P \\ \alpha_l \Delta P \end{bmatrix}. \quad (1.8)$$

Therefore, the mass flux and momentum flux for each scheme can be defined as follows

- AUSMV*:

$$(\rho \alpha V)_{j+1/2} = (\rho \alpha)_L \Omega^+(V_L, c_{j+1/2}, \chi_L) + (\rho \alpha)_R \Omega^-(V_R, c_{j+1/2}, \chi_R) \quad (1.9)$$

$$(\rho \alpha V^2)_{j+1/2} = (\rho \alpha V)_L \Omega^+(V_L, c_{j+1/2}, \chi_L) + (\rho \alpha V)_R \Omega^-(V_R, c_{j+1/2}, \chi_R) \quad (1.10)$$

- AUSMD*:

$$(\rho \alpha V)_{j+1/2} = (\rho \alpha)_L \Omega^+(V_L, c_{j+1/2}, \chi_L) + (\rho \alpha)_R \Omega^-(V_R, c_{j+1/2}, \chi_R) \quad (1.11)$$

$$(\rho \alpha V^2)_{j+1/2} = \frac{1}{2} (\rho \alpha V)_{j+1/2} (V_L + V_R) - \frac{1}{2} |(\rho \alpha V)_{j+1/2}| (V_R - V_L) \quad (1.12)$$

with

$$\Omega^\pm(V, c, \chi) = \begin{cases} \chi V^\pm(v, c) + (1 - \chi) \frac{V \pm |V|}{2} & \text{if } |V| \leq c \\ \frac{1}{2} V \pm |V| & \text{otherwise} \end{cases} \quad (1.13)$$

$$V^\pm(V, c) = \begin{cases} \pm \frac{1}{4c} (V \pm c)^2 & \text{if } |V| \leq c \\ \frac{1}{2} V \pm |V| & \text{otherwise} \end{cases} \quad (1.14)$$

and a common sound velocity

$$c_{j+1/2} = \max(c_j, c_{j+1}) \quad (1.15)$$

and

$$\chi_L = (1 - \phi_L) \frac{2(\rho/\alpha)_L}{(\rho/\alpha)_L + (\rho/\alpha)_R} + \phi_L \quad (1.16)$$

$$\chi_R = (1 - \phi_R) \frac{2(\rho/\alpha)_R}{(\rho/\alpha)_L + (\rho/\alpha)_R} + \phi_R \quad (1.17)$$

with ϕ a smooth symmetric function designed to be equal to 1 near single-phase region and 0 elsewhere. We have chosen:

$$\phi = \exp(-\kappa_1 \alpha_g) + \exp(-\kappa_2 (1 - \alpha_g)) \quad (1.18)$$

with κ_1, κ_2 are constants to determine and represent the degree of smoothness of ϕ . We choose $\kappa_1 = \kappa_2 = 200$.

The pressure terms are written as:

$$F_{j+1/2}^P = (\alpha \Delta P)_{j+1/2} = P^+(V_j, c_{j+1/2})(\alpha \Delta P)_j + P^-(V_{j+1}, c_{j+1/2})(\alpha \Delta P)_{j+1} \quad (1.19)$$

with

$$P^\pm(V, c) = V^\pm(V, c) \cdot \begin{cases} \frac{1}{c} \left(-\frac{V}{c} \pm 2\right) & \text{if } |V| \leq c \\ \frac{1}{V} & \text{otherwise} \end{cases} \quad (1.20)$$

The AUSMD* is based on matrix calculations whereas AUSMV* is characterised by scalar calculations. AUSMV* is shown to be more efficient than AUSMD* and outstandingly stable. AUSMD* is able to resolve discontinuities with more accuracy; however it tends to produce instabilities or overshoots. Hence we choose to use a hybrid scheme. AUSMDV* combines both schemes. The convective flux reads:

$$F_c^{AUSMDV^*} = s F_c^{AUSMV^*} + (1-s) F_c^{AUSMD^*} \quad (1.21)$$

with $s = \max(\phi_L, \phi_R)$, and ϕ given above in Eq. 1.18.

This choice of s makes the combined scheme to get the stability of the FVS-like scheme and the accuracy of the AUSMD* scheme.

4 NUMERICAL SIMULATIONS

4.1 Riemann shock-tubes

These test-cases are particularly chosen to test the numerical scheme's ability to handle initial data when removed from an equilibrium state. It ensures the scheme's convergence to the same weak solutions when discontinuities in volume fraction and pressure are present.

4.1.1 Toumi's problem

The initial solution of the shock-tube problem is composed by two uniform states separated by a discontinuity which is usually located at the origin. The pipe is 10m long with a diameter of 1m. The initial left and right uniform states are usually introduced by giving the density, the pressure and the velocity. This initial set represents a tube where the left and the right regions are separated by a diaphragm, and filled by the same mixture in two different physical states, with a strong disequilibrium in terms of pressure field. At $t = 0$, the discontinuity between the two initial states breaks into leftward and rightward moving waves, which are separated by a contact surface. Each wave pattern is composed by a contact discontinuity in the middle, and a shock or a rarefaction wave at the left and the right sides separating uniform state solution.

4.1.1.1 Initial and boundary conditions

The problem initial conditions read for the left and the right states:

$$\begin{aligned}
 \alpha_g^L &= 0.25 & \alpha_g^R &= 0.1 \\
 V_g^L &= 0 \text{ m.s}^{-1} & V_g^R &= 0 \text{ m.s}^{-1} \\
 V_l^L &= 0 \text{ m.s}^{-1} & \text{and } V_l^R &= 0 \text{ m.s}^{-1} \\
 P_g^L &= 2 \times 10^7 \text{ Pa} & P_g^R &= 1 \times 10^7 \text{ Pa} \\
 T^L &= 308.15 \text{ K} & T^R &= 308.15 \text{ K}
 \end{aligned}
 \tag{1.22}$$

The boundary conditions are open at both inlet and outlet of the pipe. The simulations are left running for 0.006 sec, with a series of meshes from 100 to 10000 cells.

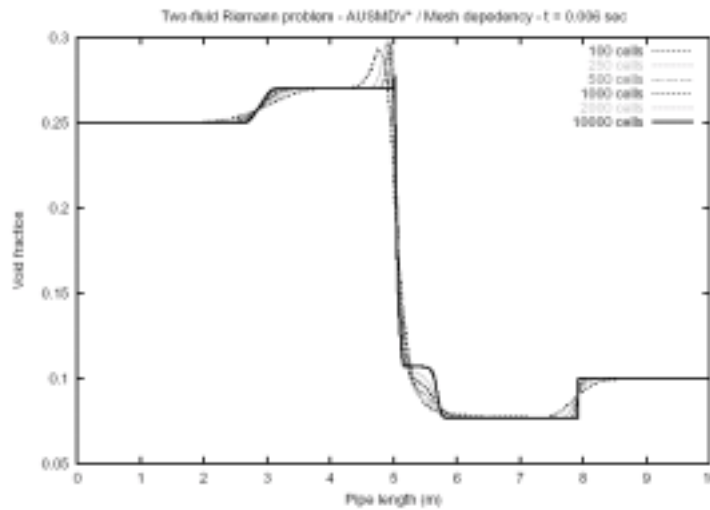


Figure 1: Toumi's Riemann air-water test-case - void fraction profile at t=0.006s, mesh dependency with AUSMDV* scheme.

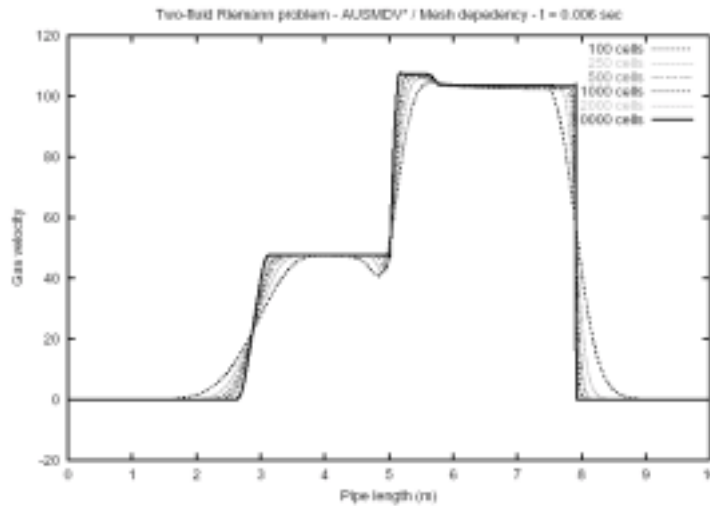


Figure 2: Toumi's Riemann Problem - gas velocity profile at t = 0.006s with AUSMDV* scheme. Diffusivity produced with coarse meshes diminishes with fine grids.

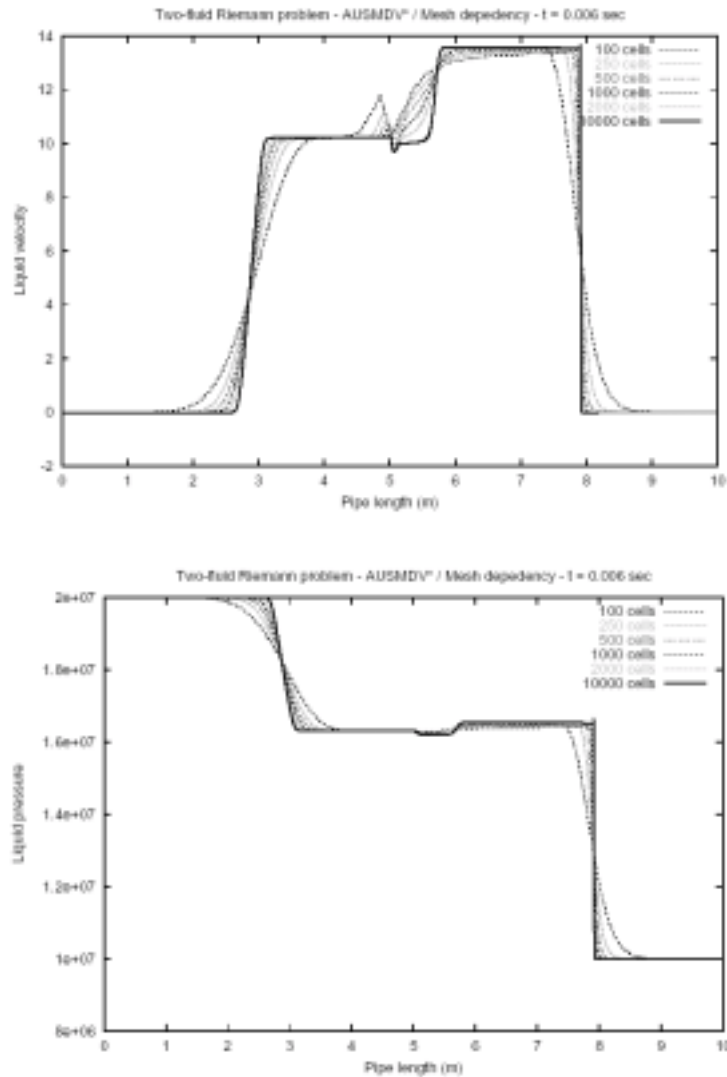


Figure 3: Toumi's Riemann Problem - mesh refinement with AUSMDV* scheme on the liquid velocity (top) and liquid pressure (bottom) profiles. Overshoots that appear around the shock ceased with mesh refinement.

4.1.1.2 Conclusion

The mesh dependency study (Fig. 1, 2 and 3) proved the convergence of the results towards the expected answer proposed in (4). Overshoots found with coarse meshes ceased with finer meshes. The simulations also captured the wave features created by the shock-tube configuration. The rarefaction, the shock-wave and the discontinuity-wave can be identified in the answers, matching with the existing results found in the literature.

Overshoots tend to appear at the shock points, such as around 5 m in the liquid velocity profile. However they are correctly decreased by the AUSMV* feature of the scheme when the mesh is refined.

4.1.2 Large relative velocity between phases

For this second two-phase Riemann problem, a large difference between the velocities is considered. The initial conditions read for the left and the right states:

$$\begin{aligned}
\alpha_g^L &= 0.29 & \alpha_g^R &= 0.3 \\
V_g^L &= 65 \text{ m.s}^{-1} & V_g^R &= 50 \text{ m.s}^{-1} \\
V_l^L &= 1 \text{ m.s}^{-1} & \text{and } V_l^R &= 1 \text{ m.s}^{-1} \\
P_g^L &= 2.65 \times 10^5 \text{ Pa} & P_g^R &= 2.65 \times 10^5 \text{ Pa} \\
T^L &= 308.15 \text{ K} & T^R &= 308.15 \text{ K}
\end{aligned}
\tag{1.23}$$

The boundary conditions are open at both inlet and outlet of the pipe. The simulations are left running for 2.0sec, with meshes from 50 to 800 cells.

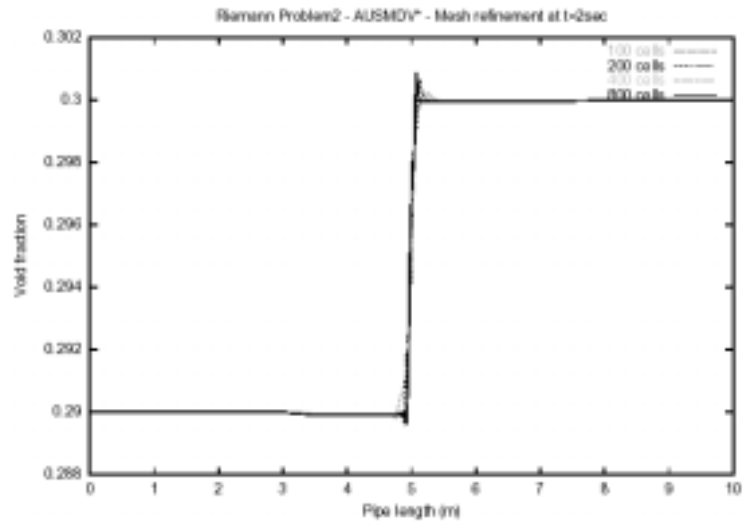


Figure 4: Riemann Problem 2 - mesh refinement with AUSMDV* results of void fraction profile at the end of the simulation.

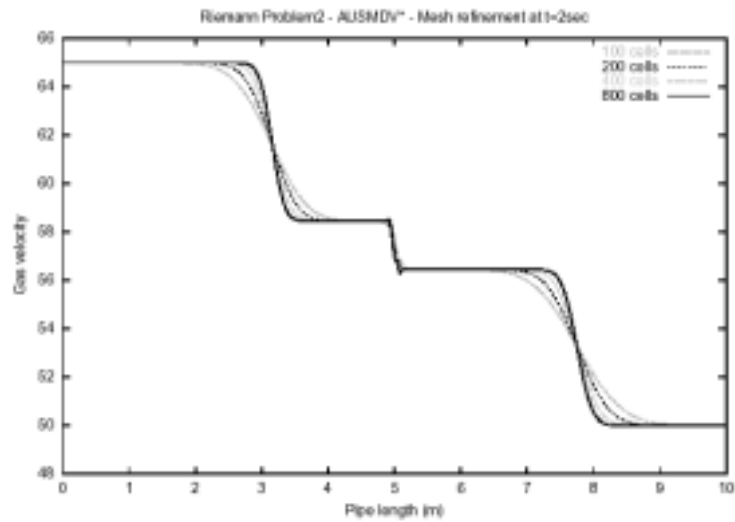


Figure 5: Riemann Problem 2 - mesh refinement study on the gas velocity profile after 2 sec.

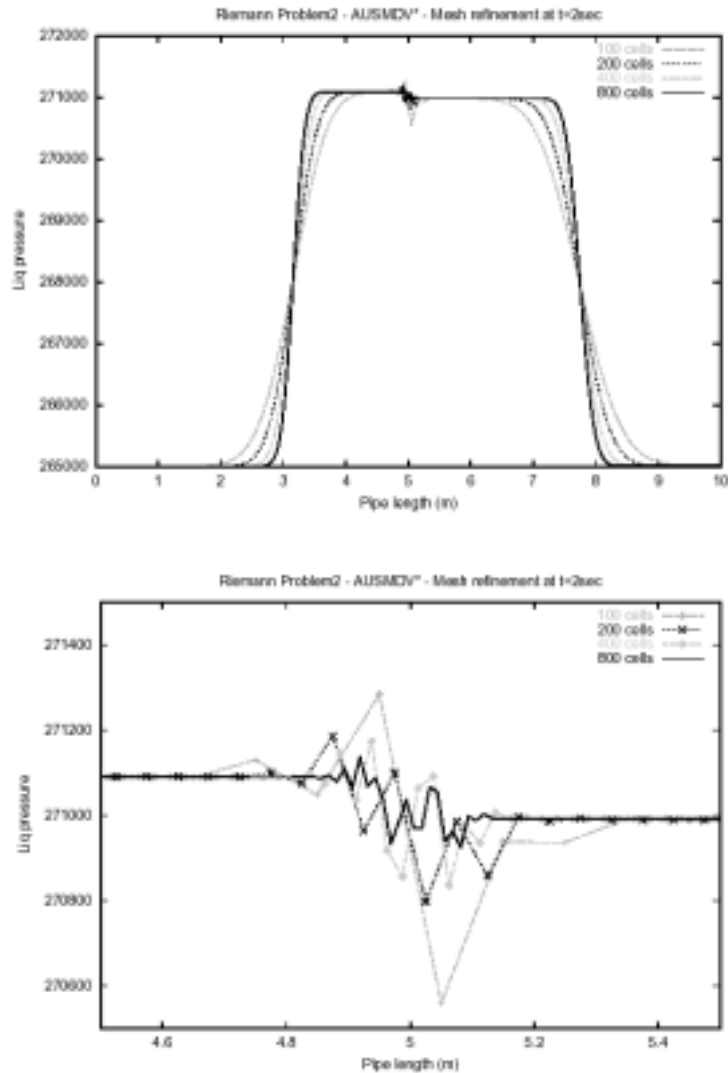


Figure 6: Riemann Problem 2 - Liquid pressure (top) and liquid pressure detailed (bottom) mesh refinement at the end of the simulation. The overshoots that appear at the shock region are reduced with finer meshes.

4.1.2.1 Analysis

From Fig. 4 and 5, we observe that mesh refinement ensures convergence of the answers for the void fraction and gas velocity profiles. It also shows the effect of a large pressure gradient at $t = 0$ that occurs and generates wiggles around the shock, as reinforced with the liquid pressure profile in Fig. 6. However a detailed result around the discontinuity at 5m for the pressure profile answer allows us to conclude that mesh refinement does control and decrease these overshoots as previously obtained in Toumi's Riemann problem.

4.2 Water faucet

The water faucet problem consists of a vertical tube 12 m in length and 1 m in diameter. The top has a fixed inflow rate of water at a velocity of $10 \text{ m}\cdot\text{s}^{-1}$, temperature of 50°C and a liquid volume fraction of 0.8. The bottom of the tube is open to the ambient pressure and the top is closed to vapor flow. The water is accelerated under gravity. The interfacial drag is set to zero. For the boundary conditions, void fraction and liquid and gas velocities are imposed equal to their initial values, and the pressure is extrapolated from the computational domain. At the outlet, all the variables are open, except the pressure, which is imposed to 10^5 Pa .

The problem allows an analytical solution, obtained with the assumptions of incompressible liquid and with the omission of pressure variation in the liquid:

$$\alpha(x,t) = \begin{cases} 1 - \frac{(1-x_0)V_{l,0}}{2} & \text{if } x \leq \frac{gt^2}{2} + V_{l,0}t \\ 0.2 & \text{else} \end{cases} \quad (1.24)$$

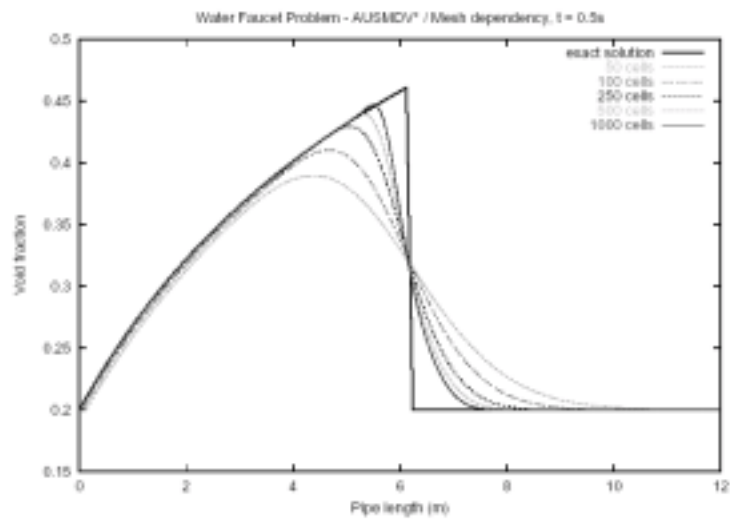


Figure 7: Mesh dependency on the void fraction profile with AUSMDV* scheme at t=0.5s. Convergence of the results is ensured.

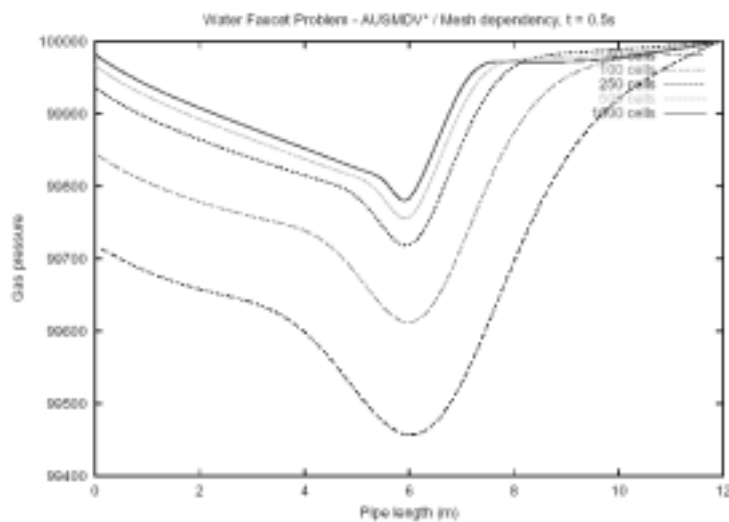


Figure 8: Water Faucet problem - gas pressure profile at t = 0.5 s, for meshes from 50 to 1000 cells.

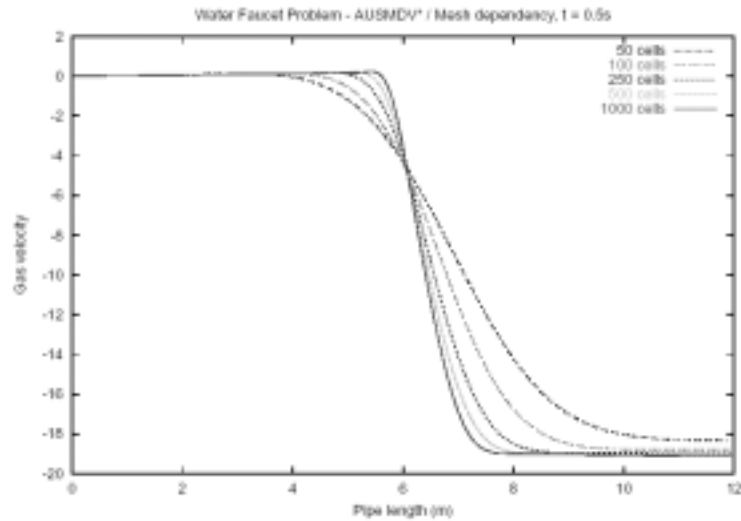


Figure 9: Water Faucet problem - gas velocity profile at $t = 0.5$ s, for meshes from 50 to 1000 cells.

4.2.1 Convergence study

Figure 7, 8 and 9 represent the profiles of gas volume fraction, pressure and velocity given by the simulations after $t = 0.5$ sec. In Fig. 7, we can see the mesh dependency effect on the void fraction at $t = 0.5$ sec with AUSMDV* scheme. Meshes from 50 cells to 1000 cells are used. As expected, refinement improves the answer. The same pattern is observed for the gas pressure (Fig. 8) and the gas velocity (Fig. 9). Table 2 shows the rate of convergence for the solution to the analytical at 5.8 m and at $t = 0.5$ sec. We compute the difference between the theoretical solution and the prediction as well as the refinement and the error ratio. We can observe that the error decreases with the mesh size.

k	Δx_k	$e_k = \alpha_{th} - \alpha_n $	$\Delta x_k / \Delta x_1$	e_k / e_1
1	0.24	0.108373	-	-
2	0.12	0.104559	0.5	0.964807
3	0.048	0.077739	0.2	0.717328
4	0.024	0.057701	0.1	0.53243
5	0.012	0.039286	0.05	0.362507
6	0.006	0.019695	0.025	0.181733
7	0.003	0.005476	0.0125	0.050529

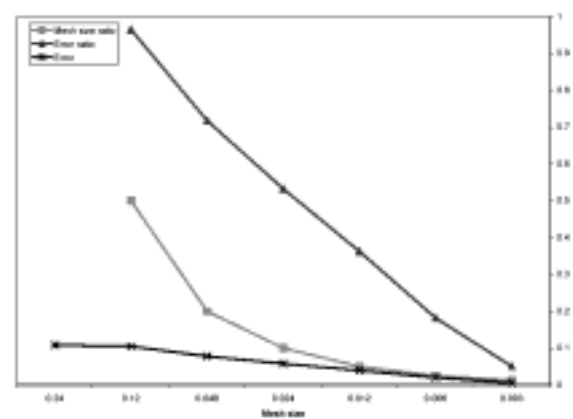


Table 2: Water Faucet Problem – error convergence at 5.8 m and at $t = 0.5$ sec.

4.3 Phase separation

This problem describes a gravity-induced phase separation in a vertical pipe. The initial homogeneous mixture consists of stagnant water and air with the same volume fraction. Both initial velocities are equal to 0. The pipe length is 7.5 m with a diameter of 1m and the

pressure is set to 1 bar. The pipe is considered to be closed at both extremities, forcing both velocities to be null at those points.

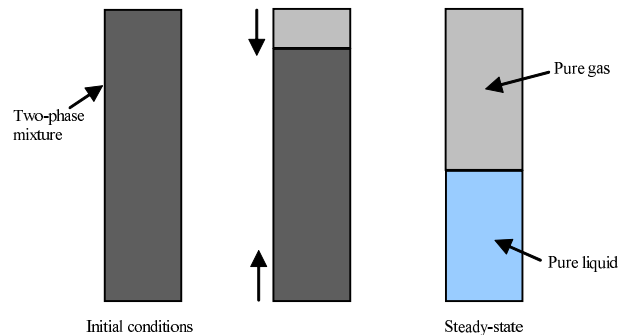


Figure 10: Phase separation problem description.

4.3.1 Convergence study

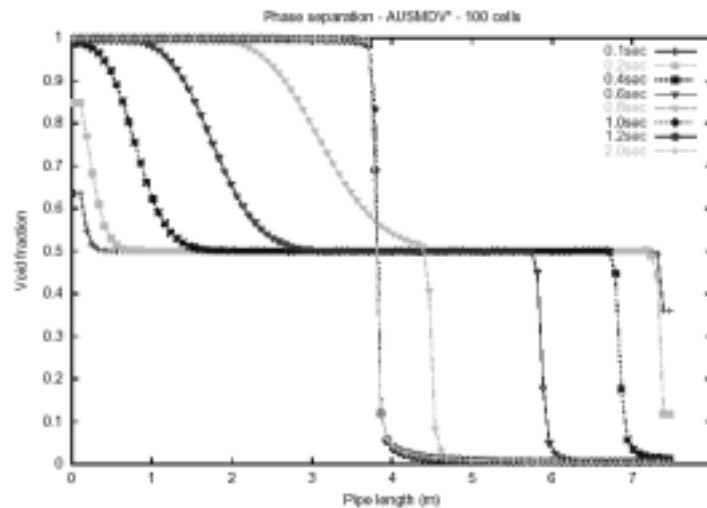


Figure 11: Void fraction profile time evolution during the simulation. After 1s, the phases are totally separated. Simulations run with AUSMDV* scheme and a mesh of 100 cells.

From Fig. 11, which shows the time evolution of the void fraction profile, the transient period reveals two volume fraction fronts at the top and the bottom of the pipe. These two fronts slowly meet and a stationary state is then formed: both phases are fully separated. This steady-state occurs after 1s, and the later volume fraction results are thus overlapping.

In Fig.12 and Fig. 13, we compare our predictions against analytical solution, obtained when assuming that the pressure variation can be neglected (3). Volume fraction and liquid velocities have hence an approximate analytical solution.

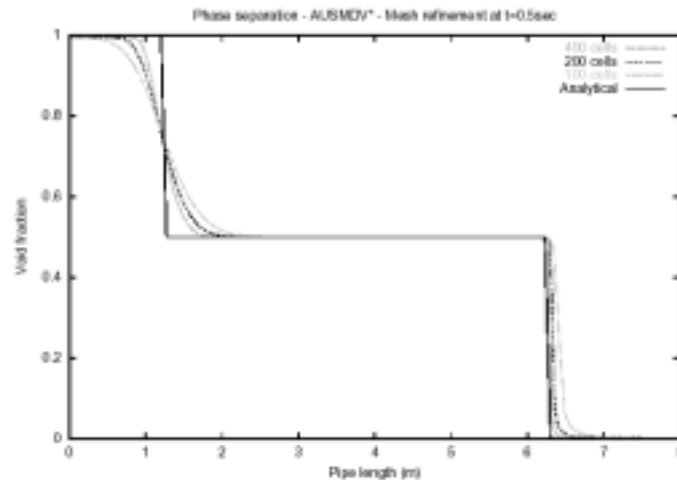


Figure 12: Two-phase separation problem - void fraction profile at $t = 0.5$ s with comparison with the analytical solution.

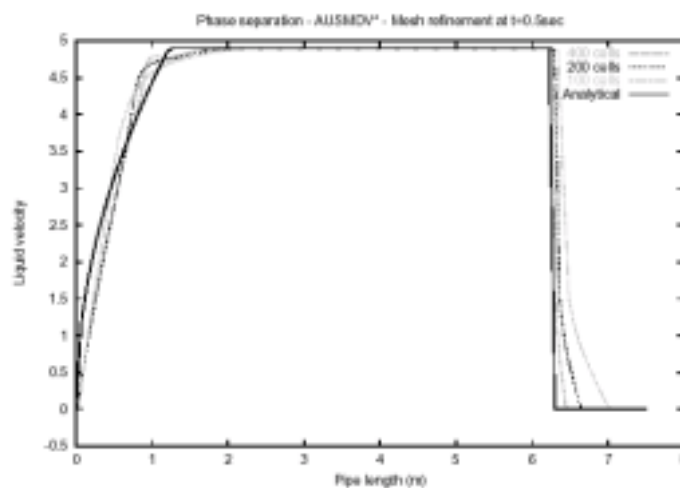


Figure 13: Two-phase separation problem - liquid velocity profile at $t=0.5$ sec, with comparison with the analytical solution.

Discontinuous waves in the void fraction profile are well handled by the scheme: the “gas” front is a little more diffusive than the “liquid” front. Transition from two-phase to one-phase region is successfully reproduced. Mesh refinement ensures the convergence of the results.

5 CONCLUSION

This paper presents numerical simulations of two-phase flow with a two-pressure, two-fluid model. Several test-cases evaluating accuracy and efficiency for the model and for the numerical methods are performed. Some typical problems occurred but mesh refinement fixes them. Therefore the features that the different tests require are all reproduced. Of course these tests are all classical benchmarks and when performing practical cases against experimental data, the validation will be more significant. However, this first stage being achieved provides a good base for future numerical experiments.

6 ACKNOWLEDGMENTS

This work has been undertaken within the Joint Project on Transient Multiphase Flows. The authors wish to acknowledge the contributions made to this project by the Engineering and Physical Sciences Research Council (EPSRC), the Department of Trade and Industry and the following: - Advantica; AspenTech; BP Exploration; ChevronTexaco; ConocoPhillips; ENI; FEESA; Granherne; Institutt for Energiteknikk; Institut Français du Pétrole; Norsk Hydro; Scandpower; Shell; SINTEF; Statoil; Total. The authors wish to express their sincere gratitude for this support.

7 REFERENCES

- (1) Saurel, R. and Abgrall, R. A Multiphase Godunov Method for Compressible Multifluid and Multiphase Flows. *J. Comp. Phys.*, **150**, 425-467 (1999).
- (2) Ransom, V.H., Hyperbolic Two-Pressure Models for Two-Phase Flow. *J. Comp. Phys.*, **53**, 124-151 (1984).
- (3) Evje, S. and Flatten, T. Hybrid flux-splitting schemes for a common two-fluid model, *J. Comp. Phys.*, **192**, 175-210 (2003).
- (4) Paillere, H., Corre, C. and Garcia Cascales, J.R. On the extension of the AUSM+ scheme to compressible two-fluid models. *Computers and Fluids*, **32**, 6, 891-916 (2003).
- (5) Niu, Y.Y. Advection upwinding splitting method to solve a compressible two-fluid model. *Int. J. Numer. Meth. Fluids*, **36**, 351-371 (2001).
- (6) Toumi, I and Kumbaro, A. An Approximate Linearized Riemann Solver for a Two-Fluid Model. *J. Comp. Phys.*, **124**, 286-300 (1996).
- (7) Stadtke H. et al. Numerical simulation of multi-dimensional two-phase flow based on flux vector splitting. *Nuclear Engineering and Design*, **177**, 199-213 (1997).
- (8) Tiselj, I and Petelin, S. Modelling of Two-Phase Flow with Second-Order Accurate Scheme. *J. Comp. Phys.*, **136**, 503-521 (1997).
- (9) Liou, M.-S. and Steffen, C.J. A New Flux Splitting Scheme, *NASA TM104404*, (1991).
- (10) Liou, M.-S. A Sequel to AUSM: AUSM+. *J. Comp. Phys.*, **129**, 364-382 (1996).
- (11) Niu, Y.Y. and Liou M.S. Numerical Simulation of Dynamic Stall using Improved Advection Upwind Splitting Method, *AIAA Journal*, **37**, 1386-1392 (Nov. 1999).
- (12) Bestion, D. The physical closure laws in the CATHARE code. *Nucl. Eng. Design*, **45**, 124-229 (1990).